

Melting relations in the MgO–MgSiO₃ system up to 70 GPa

Satoka Ohnishi¹ · Yasuhiro Kuwayama^{1,2} · Toru Inoue¹

Received: 17 September 2016 / Accepted: 7 January 2017 / Published online: 2 February 2017
© Springer-Verlag Berlin Heidelberg 2017

Abstract Melting experiments in a binary system MgO–MgSiO₃ were performed up to 70 GPa using a CO₂ laser heated diamond anvil cell. The quenched samples were polished and analyzed by a dualbeam focused ion beam (FIB) and a field emission scanning electron microscope (FE-SEM), respectively. The liquidus phase and the eutectic composition were determined on the basis of textural and chemical analyses of sample cross sections. Our experimental results show that the eutectic composition is the Si/Mg molar ratio of ~0.76 at 35 GPa and it decreases with increasing pressure. Above 45 GPa, it becomes relatively constant at about 0.64–0.65 Si/Mg molar ratio. Using our experimental data collected at a wide pressure range up to 70 GPa together with previous experimental data, we have constructed a thermodynamic model of the eutectic composition of the MgO–MgSiO₃ system. The eutectic composition extrapolated to the pressure and temperature conditions at the base of the mantle is about 0.64 Si/Mg molar ratio. The modeled eutectic composition is quite consistent with a previous prediction from ab initio calculations (de Koker et al. in *Earth Planet Sci Lett* 361:58–63, 2013), suggesting that the simple assumption of a non-ideal regular solution model can well describe the melting relation of the MgO–MgSiO₃ system at high pressure. Our results show that the liquidus phase changes from MgO-periclase to MgSiO₃-bridgmanite at 35 GPa for the

simplified pyrolite composition (~0.7 Si/Mg molar ratio), while MgSiO₃-bridgmanite is the liquidus phase at the entire lower mantle conditions for the chondritic composition (~0.84 Si/Mg molar ratio).

Keywords Lower mantle · Melting · Eutectic composition · Bridgmanite · High pressure · Diamond anvil cell

Introduction

Melting relations of lower mantle materials have important implications for the chemical evolution of the Earth. The moon-forming giant impact would have completely melted the Earth's mantle (Canup 2004), forming the global magma ocean. The freezing process from the global magma ocean may have produced chemical differentiation in the mantle. In the present Earth, seismological studies reported the presence of ultra-low velocity zones (ULVZs) near the core-mantle boundary (CMB), which have strong reductions in seismic velocities (in the range of 10–30%) for both P and S waves (e.g. Wen and Helmberger 1998; Garnero and Helmberger 1998). Partial melting of lower mantle materials has been proposed to explain the ULVZs (e.g. Williams and Garnero 1996; Lay et al. 2004), but validation about the nature of the ULVZ remains challenging. Melting relations of lower mantle materials are a key to understanding the crystallization process of the global magma ocean and the nature of the ULVZs. While melting relations of mantle materials at upper mantle pressure conditions have been studied on various compositions using a multi-anvil apparatus (e.g. Ohtani 1979, 1987; Takahashi 1986; Inoue 1994; Ito et al. 2004; Litasov and Ohtani 2002, 2005), melting experiments at higher pressures corresponding to

✉ Satoka Ohnishi
ohnishi@sci.ehime-u.ac.jp

¹ Geodynamics Research Center, Ehime University, 2-5 Bunkyo-cho, Matsuyama, Ehime 790-8577, Japan

² Present Address: Department of Earth and Planetary Science, Tokyo University, 7-3-1 Hongo, Bunkyo-ku, Tokyo 113-0033, Japan

lower mantle conditions are still limited. Only a few model rock compositions, such as peridotite and mid-oceanic ridge basalt (MORB), were studied under CMB conditions using a laser heated diamond anvil cell (LHDAC) (e.g. Fiquet et al. 2010; Nomura et al. 2011; Tateno et al. 2014; Andraut et al. 2014). The difference in bulk chemical compositions of the mantle has a large effect on the melting behavior such as the appearance of the liquidus phase and the degree of melting (e.g. Inoue 1994; Boukaré et al. 2015). The melting phase diagram as a function of pressure and composition are fundamental to understanding the melting relations of the lower mantle. For melting relations in the binary system MgO–MgSiO₃, which is a major component in the lower mantle, melting experiments have been performed up to only 26 GPa (Taylor 1973; Chen and Presnall 1975; Kato and Kumazawa 1985, 1986; Presnall and Gasparik 1990; Liebske and Frost 2012).

Here, we carried out melting experiments on the MgO–MgSiO₃ system up to 70 GPa by LHDAC experiments and chemical analyses of the recovered samples using an FE-SEM. On the basis of the melting texture and the chemical composition, we investigated the eutectic composition as a function of pressure.

Experimental procedures

Glasses of several different compositions in the MgO–MgSiO₃ system (from 0.59 to 0.91 Si/Mg molar ratios) were used as the starting material. The glasses were prepared using containerless processing with a CO₂ laser at University of Tokyo and SPring-8 (e.g. Kohara et al. 2011). In containerless processing, the materials are levitated in air during laser heating to avoid crystal nucleation. X-ray diffraction (XRD) measurements of the glasses showed that crystallization did not occur. Additionally, energy dispersive X-ray spectrometry (EDS) analyses showed the homogeneous chemical composition of the glasses.

High pressure and high temperature conditions were generated using a LHDAC. We used a symmetric type DAC. The culet size of diamond anvils was 300 μm in diameter. We pre-indented Re gaskets to about 50 μm thickness and then made a hole with 100 μm in diameter at the center. We performed melting experiments using Ar as the thermal insulator. A sample with a thickness of about 30 μm was loaded in the sample chamber and then Ar was loaded using a cryogenic technique. We also performed a few experiments without Ar at ~35 GPa to confirm whether the thermal insulator affects the melting relation or not, which showed that Ar did not affect the results. Pressures were measured at room temperature by the Raman shift of the diamond (Akahama and Kawamura 2004) before and after heating. Previous *in situ* XRD studies using a laser

heated diamond anvil cell (e.g. Fiquet et al. 2010; Nomura et al. 2014) reported that the pressure at high temperature increases due to thermal effect. In accordance with previous experiments at similar conditions, we made a correction of the thermal effect of +15% to the pressure at room temperature. The differences in the pressures before and after heating were less than 2 GPa. The pressure uncertainty is estimated to be a maximum of ±20%, which comes from differences in the samples, the cell assemblies, the experimental temperatures, and the deformation of the sample chamber with heating.

The sample was heated by a CO₂ laser installed at the Geodynamics Research Center, Ehime University, Japan (Kimura et al. 2014). A CO₂ laser with wavelength of about 10 μm can directly heat transition metal-free silicate materials such as in the MgO–MgSiO₃ system. Temperatures of the sample were measured by the spectroradiometric method. The emission spectrum was fitted in the wavelength range from 550 to 750 nm. We measured the temperature distribution across the laser heating spot. By comparing the optical image of the sample after heating and the secondary electron image of the recovered sample cross section at the center of the heating spot, we determined the temperature at the position of the boundary between solid and liquid. The temperature uncertainty is ±150 K, which is the error from the wavelength range using the fitting.

The samples were heated for about 1 s to avoid chemical segregation, which is the same as in previous experiments (e.g. Nomura et al. 2011; Tateno et al. 2014). Diffusion coefficients of Mg, Si and O in liquid have been calculated in de Koker et al. (2009). They reported that the diffusion coefficient of Si, which is the slowest species, is about 1.5×10^{-9} m²/s at 70 GPa and 4000 K. Using Fick's second law, the region of equilibrium in 1 s of about 25 μm in diameter is larger than the size of the melt pockets. While the diffusion coefficients in solids are smaller than those in liquids, the liquidus phase contacted with the liquid should attain chemical equilibrium.

The recovered samples were polished with a dualbeam FIB (FEI Scios). The texture and the chemical compositions in the cross sections of the recovered samples were analyzed using an FE-SEM (JEOL JSM-7000F) with acceleration voltages of 5–15 kV and beam currents of 1–3 nA.

Results

We determined the liquidus phase on the basis of the chemical and textual analyses in the cross section of the recovered samples. In the first run (run #1), a glass of 0.827(2) Si/Mg molar ratio was heated at 33 GPa to about 3050 K. After the pressure was released, the recovered sample was polished and analyzed (Fig. 1). Crystal growths of MgO

33 GPa, 3050 K

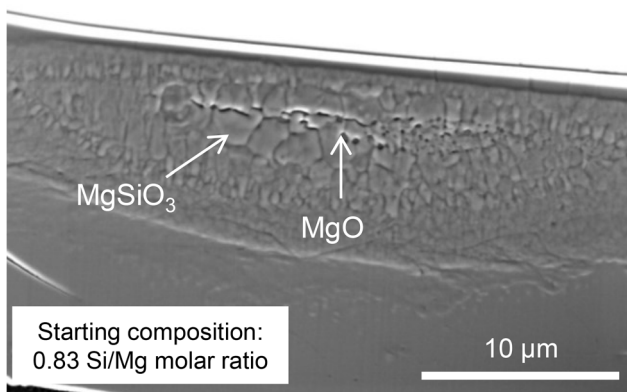


Fig. 1 A secondary electron image for the sample recovered at 33 GPa and 3050 K. The sample was heated from the *upper side*. The starting composition was 0.83 Si/Mg molar ratio. Grain growths of MgO and MgSiO₃ were observed in the center of the heated area

and MgSiO₃ were observed in the center of the hot spot. In the second run (run #2), a sample of the same composition to run #1 (0.827(2) Si/Mg molar ratio) was heated to 3950 K at 35 GPa. Figure 2a shows a secondary electron image and elemental maps for Mg and Si of the sample cross section. A quenched melt pocket with a round shape was observed at the center of the heated spot. Similar textures were observed in previous melting experiments on peridotite and MORB in DACs (e.g. Nomura et al. 2011; Tateno et al. 2014; Pardhan et al. 2015). The melt pocket was surrounded by MgSiO₃, indicating that MgSiO₃ was the liquidus phase. On the other hand, when a glass with a Si/Mg molar ratio of 0.756(5) was heated at similar *P-T* conditions (run #3), the melting texture was surrounded by an MgO layer, indicating that the liquidus phase was MgO (Fig. 2b). We also measured melt compositions in several runs (Table 1).

Our experimental results are summarized in Fig. 3. In this study, the eutectic composition was determined by two

Fig. 2 Secondary electron images (SEI) and elemental maps for Mg and Si of samples at 35 GPa. The samples were heated from the *upper side* at about 4000 K. **a** The starting composition is 0.83 Si/Mg molar ratio. The melting texture is surrounded by MgSiO₃. **b** The starting composition is 0.76 Si/Mg molar ratio. The melting texture is surrounded by an MgO layer

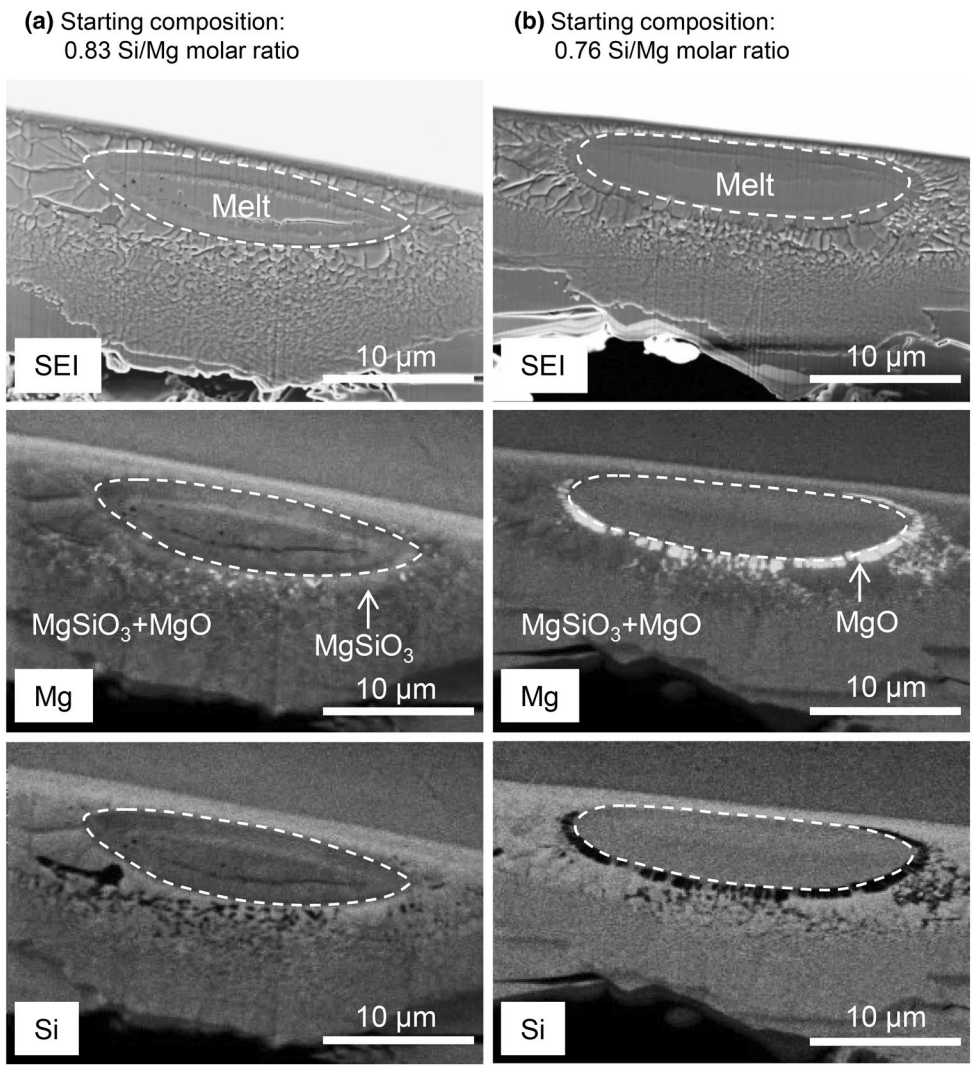


Table 1 Experimental conditions, liquidus phases and melt conditions

Run	Pressure (GPa)	Temperature (K)	Starting composition Si/Mg molar ratio	Liquidus phase	Melt composition Si/Mg molar ratio	Thermal insulator
#1	33	3050	0.827(2)	– ^b	– ^b	None
#2	35	3950	0.827(2)	MgSiO ₃	– ^c	None
#3	35	3900	0.756(5)	MgO	– ^c	None
#4	35	– ^a	0.911(4)	MgSiO ₃	0.768(8)	None
#5	35	3800	0.693(5)	MgO	0.756(20)	None
#6	35	4000	0.827(2)	MgSiO ₃	0.754(9)	Ar
#7	35	– ^a	0.756(5)	MgO	– ^c	Ar
#8	45	– ^a	0.756(5)	MgSiO ₃	0.661(20)	Ar
#9	46	2600	0.636(11)	– ^b	– ^b	Ar
#10	56	3500	0.636(11)	MgO	– ^d	Ar
#11	59	– ^a	0.589(4)	MgO	– ^d	Ar
#12	61	5150	0.693(5)	MgSiO ₃	– ^d	Ar
#13	68	3150	0.636(11)	– ^b	– ^b	Ar
#14	69	3950	0.693(5)	MgSiO ₃	0.654(31)	Ar
#15	70	4250	0.636(11)	MgO	– ^d	Ar

Parentheses show the standard deviations from several EDS measurements

^aTemperature was not measured because heating duration was too short

^bSamples were not melted

^cSamples were lost before measurements of melt compositions

^dThe melt composition was not measured because the melt pocket was too small

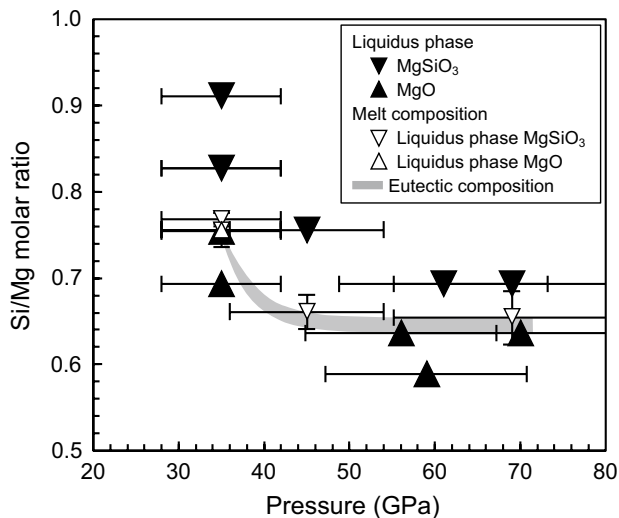


Fig. 3 The experimental results and the eutectic composition of the system MgO–MgSiO₃ as a function of pressure. The solid downward and upward triangles represent the composition of the starting material and which of MgSiO₃ or MgO, respectively, was observed as the liquidus phase. These provide the upper and lower bounds of the eutectic composition. Open downward (upward) triangles represent the composition of the melt coexisting with MgSiO₃ (MgO) as the liquidus phase. The eutectic composition (shaded area) should be located between upward and downward triangles (see text)

approaches: the change of the liquidus phase using different composition starting materials and the EDS measurements of the melt composition if the size of the melt is large enough to measure. The change of the liquidus phase depends on whether the Si/Mg molar ratio of the starting composition is larger or smaller than the eutectic composition. We prepared homogeneous starting glasses having various compositions to bracket the eutectic composition by the liquidus phase. In addition, we measured melt compositions of several recovered samples by EDS analysis (Table 1). In the present experiments, the compositions in the quenched melt pockets were quite homogeneous.

At 35 GPa, when the composition of the starting material was 0.827(2) Si/Mg molar ratio, the observed liquidus phase was MgSiO₃ (run #2 and #6) (Fig. 2a). In contrast, when the composition of the starting material was 0.756(5) Si/Mg molar ratio, the liquidus phase was MgO (run #3 and #7) (Fig. 2b). These results indicate that the eutectic composition at 35 GPa should be located between ~0.76 and ~0.83 Si/Mg molar ratio. In addition, the compositions of the melt coexisting with MgSiO₃ in run #6 and with MgO in run #5 were 0.754(9) and 0.756(20) Si/Mg molar ratio, respectively. These results suggest that the eutectic composition at 35 GPa should be about 0.76 Si/Mg molar ratio.

At 45 GPa, the liquidus phase for the starting composition of 0.756(5) Si/Mg molar ratio was MgSiO₃ and the composition of the melt coexisting with MgSiO₃ was 0.661(20) Si/Mg molar ratio (run #8). These results suggest

Table 2 Thermodynamic properties of MgO and MgSiO₃ liquids

	MgO liquid	MgSiO ₃ liquid
T_0 (K)	3000	1773
V_0 (cm ³ /mol)	16.46	37.2
K_0 (GPa)	34.0	27.3
K'	4.5	5.7
γ_0	0.96	0.6
γ'	-0.37	-1.24
C_v (kJ/K/mol)	56×10^{-3}	173×10^{-3}
S_0 (kJ/K/mol)	173.5×10^{-3}	333×10^{-3}
F_0 (kJ/mol)	-852.49	-1716.03

The parameters used are the same as Liebske and Frost (2012) expect for F_0

that the eutectic composition at 45 GPa is smaller than about 0.66 Si/Mg molar ratio.

In the same way, the eutectic composition at 56 GPa should be larger than 0.636(11) Si/Mg molar ratio (run #10) and that at 61 GPa should be smaller than 0.693(5) Si/Mg molar ratio (run #12). At about 70 GPa, the liquidus phase for the starting composition of 0.693(5) Si/Mg molar ratio was MgSiO₃ (run #14), whereas that for the starting composition of 0.636(11) was MgO (run #15). The composition of the melt coexisting with MgSiO₃ was 0.654(31) Si/Mg molar ratio (run #14). Thus, the eutectic composition at about 70 GPa should be between ~0.64 and ~0.65 Si/Mg molar ratio. The results show that the eutectic composition becomes MgO-rich with increasing pressure and becomes almost constant above 45 GPa.

Discussion

Assuming an ideal solution, when the dT/dP slope of MgO is smaller than that of MgSiO₃, the eutectic composition becomes MgO-rich with increasing pressure. While the eutectic composition determined in this study becomes MgO-rich with increasing pressure, a number of previous studies suggested that the dT/dP slope of MgO was not smaller and becomes even larger than that of MgSiO₃ with increasing pressure (e.g. Shen and Lazor 1995; Mosenfelder et al. 2009; Alfe 2005; Belonoshko and Dubrovinsky 1996; Cohen and Gong 1994; Zhang and Fei 2008; Du and Lee 2014), implying that the MgO–MgSiO₃ system cannot be described by an ideal solution. Therefore, we analyzed our experimental data with an assumption of a non-ideal regular solution by the same method with Liebske and Frost (2012), who also analyzed their data below 26 GPa and extrapolated the eutectic composition to the CMB pressure. To make a better description of the behavior of the eutectic composition under high pressure, we reanalyzed it

using higher pressure data obtained in this study in addition to the data reported in the previous study (Liebske and Frost 2012). To analyze the eutectic composition, we first calculated the pressure and temperature dependence of the chemical potentials of MgO and MgSiO₃ both in liquid (μ_{MgO}^L and $\mu_{MgSiO_3}^L$) and solid (μ_{MgO}^S and $\mu_{MgSiO_3}^S$) states based on the thermodynamic model proposed by previous studies (de Koker and Stixrude 2009; Stixrude and Lithgow-Bertelloni 2011). Details on the method are available in Liebske and Frost (2012). All parameters used are summarized in Tables 2 and 3. Using those thermodynamic parameters, we calculated the eutectic compositions under pressure. For a regular solution, the excess chemical potential can be expressed as

$$\mu_{MgO}^S - \mu_{MgO}^L = RT \ln(X_{MgO}) + (1 - X_{MgO})^2 W_{MgO-MgSiO_3} \quad (1)$$

where X_{MgO} and $W_{MgO-MgSiO_3}$ are the mole fraction of MgO of the eutectic composition of the MgO–MgSiO₃ system and the Margules interaction parameter for a given pressure and temperature, respectively. $W_{MgO-MgSiO_3}$ at each pressure and temperature was first calculated using our results and previous experimental data (Liebske and Frost 2012) and then fitted using an empirical expression, $W_{MgO-MgSiO_3} = A + \frac{B}{P}$, which is the same as Liebske and Frost (2012), where P represents pressure in units of GPa and A and B are fitting parameters. Finally, we calculated X_{MgO} as a function of pressure using $W_{MgO-MgSiO_3}$. The least-squares fit of our experimental data together with the previous data by Liebske and Frost (2012) yields $A = -42(6)$ kJ/mol and $B = 303(141)$ kJ GPa/mol. Figure 4 shows the Si/Mg molar ratio ($=1 - X_{MgO}$) of the eutectic composition as a function of pressure. To estimate the uncertainty of the prediction, we performed Monte Carlo simulations by randomly varying X_{MgO} , P and T within their absolute range of uncertainties, the same as the

Table 3 Thermodynamic properties of MgO (periclase) and MgSiO₃ (bridgmanite)

	MgO periclase	MgSiO ₃ bridgmanite
T_0 (K)	300	300
V_0 (cm ³ /mol)	11.24	24.45
K_0 (GPa)	164	251
K'	3.9	4.1
γ_0	1.36	1.57
q	1.7	1.1
Θ_0 (K)	767	905
F_0 (kJ/mol)	-569	-1368

The parameters used are the same as Liebske and Frost (2012)

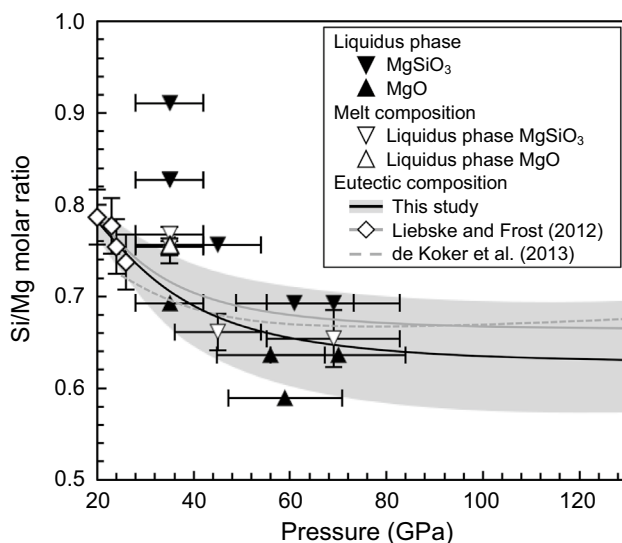


Fig. 4 A thermodynamic model of the eutectic composition of the MgO–MgSiO₃ system determined in this study (*black line*). The *shaded area* shows the model uncertainty of the eutectic composition (see text). The *solid and open triangles* represent our experimental results as described in Fig. 3. *Open diamonds* represent the eutectic composition determined by multi-anvil experiments (Liebske and Frost 2012). The *gray solid line* represents the eutectic composition proposed by Liebske and Frost (2012) based on thermodynamic modeling using their experimental data. The *gray dashed line* represents the eutectic composition proposed by ab initio calculations (de Koker et al. 2013)

previous study (Liebske and Frost 2012). We found that the uncertainty converged well within 500 simulations at each pressure. The obtained uncertainty of the molar ratio is less than ~10% under the whole lower mantle conditions (Fig. 4). From these thermodynamic considerations, the eutectic composition was constrained up to deep mantle conditions, in which the pressure range of extrapolation is smaller than the previous study.

Figure 4 also shows the comparison of the eutectic composition in the MgO–MgSiO₃ system with previous results (Liebske and Frost 2012; de Koker et al. 2013). The experimental study using a multi-anvil apparatus (Liebske and Frost 2012) reported that the eutectic composition is 0.74 Si/Mg molar ratio at 26 GPa, consistent with our experimental results at 35 GPa within experimental error. The thermodynamic model of the eutectic composition obtained in this study using experimental data collected at a much wider pressure range than the previous study is quite consistent with both the previous thermodynamic model obtained from low-pressure data (Liebske and Frost 2012) and a prediction from ab initio calculations (de Koker et al. 2013), suggesting that the simple assumption of a non-ideal regular solution model can well describe the melting relations of the MgO–MgSiO₃ system at high pressure.

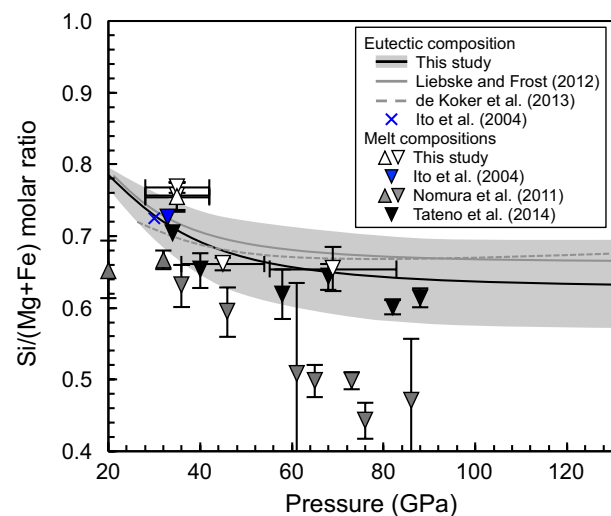


Fig. 5 The comparison with previous experiments on more complex systems. *Open triangles* represent our experimental results on the MgO–MgSiO₃ binary system as described in Figs. 3 and 4. *Lines* represent the eutectic composition of the MgO–MgSiO₃ binary system proposed by this study, Liebske and Frost (2012) and de Koker et al. (2013). The *shaded area* indicates the model uncertainty of the eutectic composition as described in Fig. 4. *Gray symbols* represent previous results of melting experiments on (Mg_{0.89}, Fe_{0.11})₂SiO₄ (Nomura et al. 2011). *Blue and black symbols* are those on peridotitic composition reported by Ito et al. (2004) and Tateno et al. (2014), respectively. *Gray, blue and black downward (upward) triangles* represent the composition of the melt coexisting with bridgmanite (ferropericlase) as the liquidus phase. *Cross*: Ito et al. (2004) also reported that the liquidus phase for peridotitic composition changes from ferropericlase to bridgmanite between 29 and 31 GPa

To understand the effect of additional chemical components on the eutectic composition, such as FeO and Al₂O₃, we also compared the present results with previous results on melting experiments of more complex systems. Figure 5 shows the composition of the melt coexisting with the liquidus phase reported in previous studies (Ito et al. 2004; Nomura et al. 2011; Tateno et al. 2014), compared with the eutectic composition of the MgO–MgSiO₃ system. Note that the compositions of the melt plotted in Fig. 5 do not indicate the eutectic composition itself but constrain the upper or lower bound of the eutectic composition (see Fig. 3). Nomura et al. (2011) performed melting experiments on (Mg_{0.89}, Fe_{0.11})₂SiO₄. They reported the change of the liquidus phase from ferropericlase (Mg, Fe)O to bridgmanite (Mg, Fe)SiO₃ at around 35 GPa, indicating that the eutectic composition of the iron-bearing system is 0.65 Si/(Mg + Fe) molar ratio at around 35 GPa, which is more SiO₂-poor than that of the MgO–MgSiO₃ binary system (about 0.70 Si/Mg molar ratio at the same pressure). Furthermore, the composition of the melt coexisting with bridgmanite as the liquidus phase becomes smaller than 0.5 Si/(Mg + Fe) molar ratio above 60 GPa, which provides

the upper bound of the eutectic composition. This also indicates that the eutectic composition of the iron-bearing system is more SiO_2 -poor than that of the iron-free system. Zhang and Fei (2008) reported that the incorporation of FeO significantly decreases the melting temperature of ferropericlase. The difference of the eutectic compositions between iron-bearing and iron-free systems might be explained by the melting temperature depression of ferropericlase since FeO is partitioned more into the liquid compared to coexisting bridgmanite (Nomura et al. 2011). For more complex compositions, Ito et al. (2004) performed melting experiments on the peridotitic composition, Si/(Mg+Fe) molar ratio of which is ~ 0.70 , showing that the liquidus phase changes from ferropericlase to bridgmanite at around 30 GPa (Fig. 5). This indicates that the eutectic composition is located at ~ 0.70 Si/(Mg+Fe) molar ratio at 30 GPa, similar to that of the MgO–MgSiO₃ binary system (this study), but more SiO_2 -rich than that of the (Mg, Fe)O–(Mg, Fe)SiO₃ system (Nomura et al. 2011). The difference of the eutectic compositions implies that the incorporation of the other components, such as Al₂O₃ and CaO, may counter the effect of FeO on the eutectic composition. This may be explained by the melting temperature depression of bridgmanite because aluminum is known to enhance the incorporation of iron into bridgmanite (e.g. Wood and Rubie 1996). Indeed, Tateno et al. (2014) reported that the melt composition of the peridotite composition coexisting with liquidus phase bridgmanite was about 0.63 Si/(Mg+Fe) molar ratio between 40 and 80 GPa, which is more SiO_2 -rich than that of the (Mg, Fe)O–(Mg, Fe)SiO₃ system (Nomura et al. 2011) but rather similar to that of the MgO–MgSiO₃ system.

Melting relations, in particular the eutectic composition and the crystallization sequence, have important implications for understanding the chemical evolution of the mantle in the early history of the Earth, since fractional crystallization of the magma ocean may have caused large chemical differentiation in the mantle. Upon fractional crystallization of the magma ocean, the composition of the residual melt should change towards its eutectic composition. The melting relations are also crucial for understanding the chemical evolution of the present mantle, since the seismically observed ULVZs have been attributed to the presence of partial melt at the base of the mantle (e.g. Williams and Garnero 1996; Lay et al. 2004). The compositional difference between the lowermost mantle and its eutectic composition may affect the degree of chemical differentiation at the base of the mantle. Though several high-pressure experiments reported the liquidus phase of several model rock compositions, such as peridotite and chondrite, at lower mantle conditions (e.g. Fiquet et al. 2010; Andraut et al. 2014; Tateno et al. 2014), their eutectic compositions are still unclear. As discussed above, both the liquidus

phase and the eutectic composition are largely affected by which components are included in the system.

In this study, we determined the eutectic composition of the most simplified binary system, MgO–MgSiO₃, for mantle material based on experimental data up to 70 GPa, corresponding to the middle of the lower mantle, and extrapolated it to the pressure at the base of the mantle on the basis of thermodynamic modeling. The results indicate that the Si/Mg molar ratio of the eutectic composition of the MgO–MgSiO₃ system decreases with increasing pressure up to about 45 GPa and becomes rather constant at about 0.64 up to the pressure at the base of the mantle (Fig. 4). For the crystallization of the magma ocean, it is still not clear at what depth the whole mantle magma ocean began to crystallize, which depends on the slopes of its liquidus and the isentropic temperature gradient. According to a recent study by Thomas et al. (2012) based on the equation of state of liquid Mg₂SiO₄ and Fe₂SiO₄ by shock-wave experiments and calculated isentropes for liquid peridotite and chondritic mantle composition, the peridotitic magma ocean would have started crystallization from the middle of the lower mantle around 2000 km depth, where the pressure is about 85 GPa, and crystallization proceeded both upward and downward, whereas the chondritic magma ocean crystallization would have started from the base of the lower mantle and proceeded upward. If the chondritic magma ocean model is the case, bridgmanite first crystallized from the base of the mantle and crystallization proceeded towards the shallower part. The composition of the remnant melt changes towards the eutectic composition. As a consequence, the composition after crystallization becomes the most SiO_2 -rich at the base, changes towards MgO-rich with decreasing depth, and becomes almost similar to the initial composition of the magma ocean at the top, since the eutectic composition changes towards SiO_2 -rich with decreasing pressure and becomes almost similar to the chondritic composition at the pressure of the upper mantle. On the other hand, if the peridotitic magma ocean model is the case, since crystallization would have started at the middle of the lower mantle and proceeded both upward and downward, the last remnant melt at the top and base of the mantle should have the most MgO-rich composition. Of course, this is too simplistic to model the actual magma ocean crystallization and the effect of other components, including FeO, Al₂O₃, CaO and so on, on the eutectic composition and the crystallization sequences should be investigated. The density contrast between the crystallizing solid and the residual melt should also be considered to understand the actual chemical evolution of the mantle (e.g. Thomas et al. 2012; Labrosse et al. 2015). As in the above discussion, the FeO component would decrease the Si/(Mg+Fe) molar ratio of the eutectic composition, but the other components might counter this effect. In addition,

the effect of volatiles such as H₂O and CO₂ on the melting relations may also be important, though it is still not clear how much these components are included in the deep mantle. Although further studies on the effect of such additional components are required, the present result on the melting relation of the MgO–MgSiO₃ system should be the baseline for a fundamental understanding of the melting relations of mantle materials.

In this study, we used a CO₂ laser heating technique to determine the melting relation of the MgO–MgSiO₃ system. Since the method does not require the addition of a metal absorber (e.g. Pt, Au) in the sample chamber nor the incorporation of a transition metal (e.g. Fe) in the sample itself, it may be useful for studying melting relations of mantle materials, particularly transition metal-free systems.

Acknowledgements We thank T. Kimura, A. Shinozaki, S. Machida, and H. Hirai for help with the development of the CO₂ laser heating system. A. Masuno and K. Ohara are acknowledged for preparation of glasses as the starting materials. We also thank H. Dekura and T. Taniuchi for calculations, S. Tateno, Y. Nakajima and R. Nomura for discussions. This study was supported in part by the Grants-in-Aid of the Scientific Research (Nos. 26247073 and 15H05828 to T. Inoue) of the Japan Society for the Promotion of Science.

References

- Akahama Y, Kawamura H (2004) High-pressure Raman spectroscopy of diamond anvils to 250 GPa: method for pressure determination in the multimegabar pressure range. *J Appl Phys* 96:3748–3751. doi:10.1063/1.1778482
- Alfe D (2005) Melting curve of MgO from first-principles simulations. *Phys Rev Lett* 94:235701. doi:10.1103/PhysRevLett.94.235701
- Andraut D, Pesce G, Bouhifd MA, Bolfan-Casanova D, Hénot JM, Mezouar M (2014) Melting of subducted basalt at core-mantle boundary. *Science* 344:892–895. doi:10.1126/science.1250466
- Belonoshko AB, Dubrovinsky LS (1996) Molecular dynamics of NaCl (B1 and B2) and MgO (B1) melting: two-phase simulation. *Am Mineral* 81:303–316. doi:10.2138/am-1996-3-404
- Boukaré CE, Ricard Y, Fiquet G (2015) Thermodynamics of the MgO–FeO–SiO₂ system up to 140 GPa: application to crystallization of Earth's magma ocean. *J Geophys Res* 120:6085–6101. doi:10.1002/2015JB011929
- Canup RM (2004) Simulation of a late lunar-forming impact. *Icarus* 168:433–456. doi:10.1016/j.icarus.2003.09.028
- Chen CH, Presnall DC (1975) The system Mg₂ SiO₄–SiO₂ at pressures up to 25 kilobars. *Am Mineral* 60:398–406
- Cohen RE, Gong Z (1994) Melting and melt structure of MgO at high pressures. *Phys Rev B* 50:12301. doi:10.1103/PhysRevB.50.12301
- de Koker N, Stixrude L (2009) Self-consistent thermodynamic description of silicate liquids, with application to shock melting of MgO periclase and MgSiO₃ perovskite. *Geophys J Int* 178:162–179. doi:10.1111/j.1365-246X.2009.04142.x
- de Koker NP, Stixrude L, Karki BB (2009) Thermodynamics, structure, dynamics, and freezing of Mg₂ SiO₄ liquid at high pressure. *Geochim Cosmochim Acta* 72:1427–1441. doi:10.1016/j.gca.2007.12.019
- de Koker N, Karki BB, Stixrude LN (2013) Thermodynamics of the MgO–SiO₂ liquid system in Earth's lowermost mantle from first principles. *Earth Planet Sci Lett* 361:58–63. doi:10.1061/j.epsl.2012.11.026
- Du Z, Lee KKM (2014) High-pressure melting of MgO from (Mg,Fe) O solid solutions. *Geophys Res Lett* 41:1–6. doi:10.1002/2014GL061954
- Fiquet G, Auzende AL, Siebert J, Corgne A, Bureau H, Ozawa H, Garbarino G (2010) Melting of peridotite to 140 gigapascals. *Science* 329:1516–1518. doi:10.1126/science.1192448
- Garnero EJ, Helmberger DV (1998) Further structural constraints and uncertainties of a thin laterally ultralow-velocity layer at the base of the mantle. *J Geophys Res* 103:12495–12509. doi:10.1029/98JB00700
- Inoue T (1994) Effect of water on melting phase relations and melt composition in the system Mg₂ SiO₄–MgSiO₃–H₂O up to 15 GPa. *Phys Earth Planet Inter* 85:237–263. doi:10.1016/0031-9201(94)90116-3
- Ito E, Kubo A, Katsura T, Walter MJ (2004) Melting experiments of mantle materials under lower mantle conditions with implications for magma ocean differentiation. *Phys Earth Planet Inter* 143–144:397–406. doi:10.1016/j.pepi.2003.09.016
- Kato T, Kumazawa M (1985) Effect of high pressure on the melting relation in the system Mg₂ SiO₄–MgSiO₃ part I. Eutectic relation up to 7 GPa. *J Phys Earth* 33:513–524. doi:10.4294/jpe.1952.33.513
- Kato T, Kumazawa M (1986) Melting and phase relation in the system Mg₂ SiO₄–MgSiO₃ at 20 GPa under hydrous conditions. *J Geophys Res* 91:9351–9355. doi:10.1029/JB091iB09p09351
- Kimura T, Kuwayama Y, Yagi T (2014) Melting temperatures of H₂O up to 72 GPa measured in a diamond anvil cell using CO₂ laser heating technique. *J Chem Phys* 140:074501. doi:10.1063/1.4865252
- Kohara S, Akola J, Morita H, Suzuya K, Weber JKR, Wilding MC, Benmore CJ (2011) Relationship between topological order and glass forming ability in densely packed enstatite and forsterite composition glasses. *Proc Natl Acad Sci* 14780–14785. doi:10.1073/pnas.1104692108
- Labrosse S, Hernlund JW, Hirose K (2015) Fractional melting and freezing in the deep mantle and implications for the formation of a basal magma ocean. In: Badro J, Walter M (eds) *The early Earth: accretion and differentiation*, AGU monograph 212. Wiley, New York, pp 123–142
- Lay T, Garnero EJ, Williams Q (2004) Partial melting in a thermochemical boundary layer at the base of the mantle. *Phys Earth Planet Inter* 146:441–467. doi:10.1016/j.pepi.2004.04.004
- Lieske C, Frost DJ (2012) Melting phase relations in the MgO–MgSiO₃ system between 16 and 26 GPa: implications for melting in Earth's deep interior. *Earth Planet Sci Lett* 345–348:159–170. doi:10.1016/j.epsl.2012.06.038
- Litasov K, Ohtani E (2002) Phase relations and melt compositions in CMAS–pyrolyte–H₂O system up to 25 GPa. *Phys Earth Planet Inter* 134:105–127. doi:10.1016/S0031-9201(02)00152-8
- Litasov KD, Ohtani E (2005) Phase relation in hydrous MORB at 18–28 GPa: implications for heterogeneity of the lower mantle. *Phys Earth Planet Inter* 150:239–263. doi:10.1016/j.pepi.2004.10.010
- Mosenfelder JL, Asimow PD, Frost DJ, Ruibe DC, Ahrens TJ (2009) The MgSiO₃ system at high pressure: thermodynamic properties of perovskite, postperovskite, and melt from global inversion of shock and static compression data. *J Geophys Res* 1(1):4. doi:10.1029/2008JB005900
- Nomura R, Ozawa H, Tateno S, Hirose K, Hernlund J, Muto S, Ishii H, Hiraoka N (2011) Spin crossover and iron-rich silicate melt in the Earth's deep mantle. *Nature* 473:199–202. doi:10.1038/nature09940

- Nomura R, Hirose K, Uesugi K, Ohishi Y, Tsuchiyama A, Miyake A, Ueno Y (2014) Low core-mantle boundary temperature inferred from the solidus of pyrolite. *Science* 343:522–525. doi:[10.1126/science.1248186](https://doi.org/10.1126/science.1248186)
- Ohtani E (1979) Melting relation of Fe_2SiO_4 up to about 200 kbar. *J Phys Earth* 27:189–208. doi:[10.4294/jpe.1052.27.189](https://doi.org/10.4294/jpe.1052.27.189)
- Ohtani E (1987) Ultrahigh-pressure melting of a model chondritic mantle and pyrolite compositions. In: Manghnai MH, Syono Y (eds) High-pressure research in mineral physics: a volume in honor of Syun-iti Akimoto. AGU, Washington D.C. doi:[10.1029/GM039p0087](https://doi.org/10.1029/GM039p0087)
- Pradhan GK, Fiquet G, Siebert J, Auzende AL, Morard G, Antonangeli D, Garbarino G (2015) Melting of MORB at core–mantle boundary. *Earth Planet Sci Lett* 431:247–251. doi:[10.1016/j.epsl.2015.09.034](https://doi.org/10.1016/j.epsl.2015.09.034)
- Presnall DC, Gasparik T (1990) Melting of enstatite (MgSiO_3) from 10 to 16.5 GPa and the forsterite (Mg_2SiO_4)–majorite (MgSiO_3) eutectic at 16.5 GPa: implications for the origin of the mantle. *J Geophys Res* 95:15771–15777. doi:[10.1029/JB095iB10p15771](https://doi.org/10.1029/JB095iB10p15771)
- Shen G, Lazor P (1995) Measurement of melting temperatures of some minerals under lower mantle pressures. *J Geophys Res* 100:17699–17713. doi:[10.1029/95JB01864](https://doi.org/10.1029/95JB01864)
- Stixrude L, Lithgow-Bertelloni C (2011) Thermodynamics of mantle minerals—II. Phase equilibria. *Geophys J Int* 184:1180–1213. doi:[10.1111/j.1365-246X.2010.04780.x](https://doi.org/10.1111/j.1365-246X.2010.04780.x)
- Takahashi E (1986) Melting of a dry peridotite KLB-1 up to 14 GPa: Implications on the origin of peridotitic upper mantle. *J Geophys Res* 91:9367–9382. doi:[10.1029/JB091iB09p09367](https://doi.org/10.1029/JB091iB09p09367)
- Tateno S, Hirose K, Ohishi Y (2014) Melting experiments on peridotite to lowermost mantle conditions. *J Geophys Res* 119:4684–4694. doi:[10.1002/2013JB010616](https://doi.org/10.1002/2013JB010616)
- Taylor HCJ (1973) Melting relations in the system $\text{MgO}-\text{Al}_2\text{O}_3-\text{SiO}_2$ at 15 kb. *Geol Soc Am Mem* 84:1335–1348. doi:[10.1130/0016-7606\(1973\)84<1335:MRITSM>2.0.CO;2](https://doi.org/10.1130/0016-7606(1973)84<1335:MRITSM>2.0.CO;2)
- Thomas CW, Liu Q, Agee CB, Asimow PD, Lange RA (2012) Multi-technique equation of state for Fe_2SiO_4 melt and the density of Fe-bearing silicate melts from 0 to 161 GPa. *J Geophys Res Solid Earth* 117:B10206. doi:[10.1029/2012JB009403](https://doi.org/10.1029/2012JB009403)
- Wen L, Helmberge DV (1998) Ultra-low velocity zones near the core–mantle boundary from broadband *PKP* precursors. *Science* 279:1701–1703. doi:[10.1126/science.279.5357.1701](https://doi.org/10.1126/science.279.5357.1701)
- Williams Q, Garnero EJ (1996) Seismic evidence for partial melt at the base of Earth's mantle. *Science* 273:1528–1530. doi:[10.1126/science.273.5281.1528](https://doi.org/10.1126/science.273.5281.1528)
- Wood BJ, Rubie DC (1996) The effect of alumina on phase transformations at the 660-kilometer discontinuity from Fe–Mg partitioning experiments. *Science* 273:1522–1524. doi:[10.1126/science.273.5281.1522](https://doi.org/10.1126/science.273.5281.1522)
- Zhang L, Fei Y (2008) Melting behavior of (Mg,Fe)O solid solutions at high pressure. *Geophys Res Lett* 35:L13302. doi:[10.1029/2008GL034585](https://doi.org/10.1029/2008GL034585)